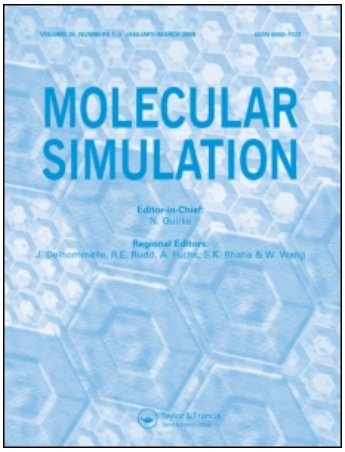

Molecular Simulation
Publication details, including instructions for authors and subscription information:
http://www.informaworld.com/smpp/title~content=t713644482

Solid-Fluid Coexistence in Binary Hard Sphere Mixtures by Semigrand Monte Carlo Simulation

David A. Kofke[a]
[a] Department of Chemical Engineering, State University of New York at Buffalo, Buffalo, NY, USA

To cite this Article Kofke, David A.(1991) 'Solid-Fluid Coexistence in Binary Hard Sphere Mixtures by Semigrand Monte Carlo Simulation', Molecular Simulation, 7: 5, 285 — 302
To link to this Article: DOI: 10.1080/08927029108022458
URL: http://dx.doi.org/10.1080/08927029108022458

Molecular Simulation, 1991, Vol. 7, pp. 285–302
Reprints available directly from the publisher
Photocopying permitted by license only

SOLID–FLUID COEXISTENCE IN BINARY HARD SPHERE MIXTURES BY SEMIGRAND MONTE CARLO SIMULATION

DAVID A. KOFKE

Department of Chemical Engineering, State University of New York at Buffalo, Buffalo, NY 14260, USA

(*Received December 1990, accepted February 1991*)

We report on Monte Carlo simulations of binary mixtures of single-occupancy hard spheres, which were conducted to evaluate coexistence with the fluid phase. The simulations were performed in a semigrand ensemble in which the temperature, pressure, total number of spheres, and fugacity fraction are independent variables, while the mixture composition and density fluctuates, and thus are averaged. Using the pure components as references, the composition averages were integrated as a function of fugacity fraction to determine the mixture free energy for comparison with the fluid phase. Three mixtures were studied, of diameter ratio $\lambda = 0.95$, 0.93, and 0.90, respectively. A spindle-type diagram is observed for the $\lambda = 0.95$ mixture, while the $\lambda = 0.93$ and $\lambda = 0.90$ mixtures each display an azeotrope. The results are in satisfactory but not complete agreement with previous simulation studies.

KEY WORDS: Solid–fluid coexistence, binary mixtures, hard spheres, semigrand Monte Carlo.

1. INTRODUCTION

The past decade has seen a great deal of activity in fundamental studies of nonuniform classical liquids in general, and liquid–solid coexistence in particular. This interest has been fueled by the success of density functional methods in characterizing the freezing transition in simple models of atomic systems [1–4]. Many variants of the density functional approach have been put forth; all share the idea of using the known thermodynamic and structural properties of a *uniform* fluid to estimate the properties of a *nonuniform* one. For sufficiently simple models, the properties of the uniform reference can be estimated accurately from standard integral equation theories. In these cases the description of solid–fluid coexistence subsequently obtained is nearly first-principles in nature — the only input is the symmetry of the nonuniform phase.

More recently, efforts have focused on phase coexistence in mixtures which, not surprisingly, has proven much more interesting [5–11]. From the density functional studies, it is now generally agreed that the simple hard sphere model with just two components exhibits a very rich phase diagram, with azeotropes, eutectics, and solid–solid immiscibility being observed. It is in this application that the various density functional methods have distinguished themselves from each other. Although they are qualitatively consistent in their predictions, they differ significantly in their quantitative conclusions, particularly concerning the effect of the sphere size ratio on the phase behavior. Recent simulation studies by Kranendonk and Frenkel [12] have

shed light on this situation, and we offer the present work to resolve further our understanding of this elementary model of freezing.

The model studied in our simulations is the substitutionally disordered binary mixture of hard spheres with centers constrained to the Wigner-Seitz (WS) cells of a fcc lattice. The sphere size distinguishes the two components, and without loss of generality we restrict the ratio of sphere diameters $\lambda = \sigma_2/\sigma_1$ to the range (0,1); thus, component 1 always refers to the species having the larger diameter. The WS cells restrain the spheres to a lattice, regardless of the mechanical or thermodynamic stability of the crystalline phase. This constraint is imposed because it allows a thermodynamic path of integration to be constructed that traverses regions in which the fluid phase is more stable. The cells — one of which is shown in Figure 1 — fill space, and one sphere is assigned to each cell. This so-called single-occupancy approach was first employed by Hoover and Ree [13] in their pioneering studies of freezing of pure hard spheres.

We present our results in terms of the reciprocal of βP, $kT/P\sigma_1^3$, which may be thought of as a temperature with the pressure held constant. We henceforth designate this quantity T^*. This is an unconventional way of describing the state of a hard sphere system, but we do it to maintain consistency with much of the literature on these mixtures.

We became aware of similar simulation studies by Kranendonk and Frenkel while nearing the completion of what is reported here. While we do not have complete details of their work, we know of several ways in which the present simulations differ from theirs. First, we simulate a much larger system: 500 spheres, instead of 108. Second, our simulations are performed in a different ensemble — the semigrand ensemble — which we believe has significant computational advantages over the canonical, constant-composition approach employed by them. With care, both methods are capable of producing the correct results, a statement which is affirmed in our direct comparison presented in Section 4. However, as discussed below, there exists a greater possibility of error when using the canonical method than when employing the semigrand. This caveat is particularly relevant to studies of solid–solid coexist-

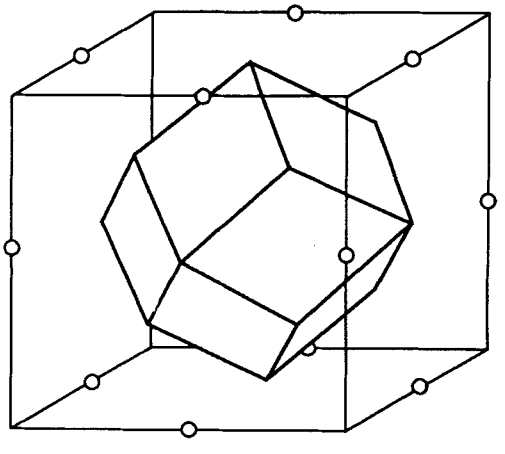

Figure 1 Wigner-Seitz cell for a face-centered-cubic lattice. The open circles represent adjacent sites on the lattice.

ence, and less to the single-occupancy approach to solid–fluid coexistence reported here, and which was not used by Kranendonk and Frenkel. Finally, we compute our phase diagrams using a semi-empirical equation of state to characterize the fluid phase; Kranendonk and Frenkel instead performed separate fluid-phase simulations to determine its properties.

This paper details the semigrand methodology as applied to freezing, describes its features, and presents our results for the thermodynamics of solid–fluid coexistence for mixtures of three size ratios λ: 0.95, 0.93, and 0.90. In particular, we do not yet present a comparison with the density functional approaches, nor do we focus on solid–solid coexistence; we reserve these issues for a future publication. In Section 2 we review the semigrand ensemble and describe how coexistence is described in this framework. In Section 3 we detail the simulations, and we report our results in Section 4. In Section 5, we discuss the results and compare them to those of Kranendonk and Frenkel. We summarize and present our conclusions in Section 6, along with a remark concerning the utility of the semigrand approach for density functional calculations.

2. THEORY

2.1 The Semigrand Ensemble

The fundamental thermodynamic equation for a binary mixture of hard spheres in the Gibbs representation may be written

$$d(\beta G) = U d\beta + V d(\beta P) + \beta\mu_1 dN + \beta(\mu_2 - \mu_1) dN_2 \tag{1}$$

Here, G is the Gibbs free energy, U, P, and V are the internal energy, pressure, and volume, μ_i and N_i are the chemical potential and number of molecules of species i, $N = N_1 + N_2$, and $\beta = 1/k_B T$, with T the temperature and k_B Boltzmann's constant. The isobaric semigrand [14] free energy is a Legendre transform of the Gibbs free energy; this potential is simply $N\beta\mu_1$

$$N\beta\mu_1 = \beta G - (\mu_2 - \mu_1)N_2 \tag{2}$$

The fundamental equation in this ensemble may be written

$$d(N\beta\mu_1) = U_\mu d\beta + V d(\beta P) + \beta\mu_1 dN - N_2 d[\beta\Delta\mu_c] \tag{3}$$

The independent variables in the isobaric semigrand ensemble are the temperature, pressure, *total* number of molecules, and the configurational chemical potential difference $\mu_{c2} - \mu_{c1}$, which we write as $\Delta\mu_c$ (the configurational chemical potential has the density independent part removed; this contribution can be combined with the $d\beta$ term, thus defining U_μ[15]). In particular, the composition is not an independent quantity. Accordingly, a simulation in this ensemble is conducted with a fixed total number of molecules, and the composition fluctuates. As described in Section 3, this sampling is achieved by allowing molecules independently to change species identities during the simulation.

The mixture composition depends on both βP and $\Delta\mu_c$. However, the imposed chemical potential difference $\Delta\mu_c$ is the thermodynamic conjugate of N_2, and thus it is the more direct means for controlling the composition. It is convenient to define an equivalent quantity, ξ_2, the fugacity fraction of species 2, which is more intuitively specified than is $\Delta\mu_c$

$$\xi_2 \equiv \frac{1}{1 + \exp(-\Delta\mu_c)} \tag{4}$$

The fugacity fraction is bounded between zero (pure species 1) and unity (pure 2), and in an ideal gas mixture it is equal to the mole fraction. When ξ_2 is introduced for $\Delta\mu_c$ in Equation (3), the fundamental equation becomes

$$d(N\beta\mu_1) = U_\mu d\beta + Vd(\beta P) + \beta\mu_1 dN - \frac{N_2}{\xi_2(1-\xi_2)} d\xi_2 \tag{5}$$

The evaluation of chemical potentials is one of the most difficult tasks encountered in molecular simulation. The advantage of the semigrand approach is that is eliminates the need to evaluate all but one of the mixture chemical potentials (regardless of the number of species in the mixture) — because $\Delta\mu_c$ is specified, knowledge of μ_1 allows μ_2 to be determined trivially. This feat is accomplished without resorting to particle insertions, which present similar difficulties. Furthermore, Equation (5) suggests a very convenient means for the evalutation of μ_1. Integration of Equation (5) at constant β, P and N results

$$\beta\mu_1(\xi_2) = \beta\mu_1^0 - \int_0^{\xi_2} \frac{x_2}{\xi_2(1-\xi_2)} d\xi_2 \tag{6}$$

where $x_2 = N_2/N$ is the species-2 mole fraction, and $\beta\mu_1^0$ is the chemical potential of *pure* species 1. Thus we can evaluate mixture properties by building upon what we already know about the pure substances. We perform a series of simulations — varying ξ_2 and measuring the composition — and integrate the results to determine the one unknown chemical potential.

The singularity in the integrand as $\xi_2 \to 1$ is unwieldy, and so we separate it from the integral

$$\beta\mu_1(\xi_2) = \beta\mu_1^0 + \ln(1-\xi_2) - \int_0^{\xi_2} \frac{x_2 - \xi_2}{\xi_2(1-\xi_2)} d\xi_2 \tag{7}$$

The integrand in this expression is well behaved for all ξ_2; its values at the extremes $\xi_2 = 0,1$ are simply related to the Henry's constants of species 2 in 1, and species 1 in 2, respectively. A complementary equation may be derived which relates μ_1 to the *pure species* 2 chemical potential, $\beta\mu_2^0$

$$\beta\mu_1(\xi_2) = \beta\mu_2^0 + \ln(1-\xi_2) + \int_{\xi_2}^{1} \frac{x_2 - \xi_2}{\xi_2(1-\xi_2)} d\xi_2 \tag{8}$$

Equations (7) and (8) allow either pure fluid to be used as a starting point. Equation (8) is particularly useful because it provides an integral consistency check of the calculations. Integration of data over the entire range of ξ_2 yields $\beta\mu_1(\xi_2 = 0)$, the chemical potential of pure component 1, which may then be compared to $\beta\mu_1^0$, if available independently.

2.2 *Evaluation of Coexistence*

Because of the small system size used in molecular simulations, phase equilibria cannot be observed directly. Direct simulations of two phase systems are dominated

by the behavior of the interface, and exhibit very large fluctuations (a notable exception is the Gibbs ensemble method of Panagiotopoulos [16]). Coexistence must instead be evaluated by strict thermodynamic criteria: equality of pressure, temperature, and all species chemical potentials between both phases. Different paradigms for conceptualizing phase coexistence can be associated with the ensembles in which the simulations are performed, and the approach taken to evaluating coexistence will vary with the ensemble used. Although these paradigms are thermodynamically equivalent, it may be found in practice that some have significant computational advantages. We will describe the semigrand paradigm for phase equilibria, but to provide contrast we first review the canonical (*i.e.*, constant composition) approach.

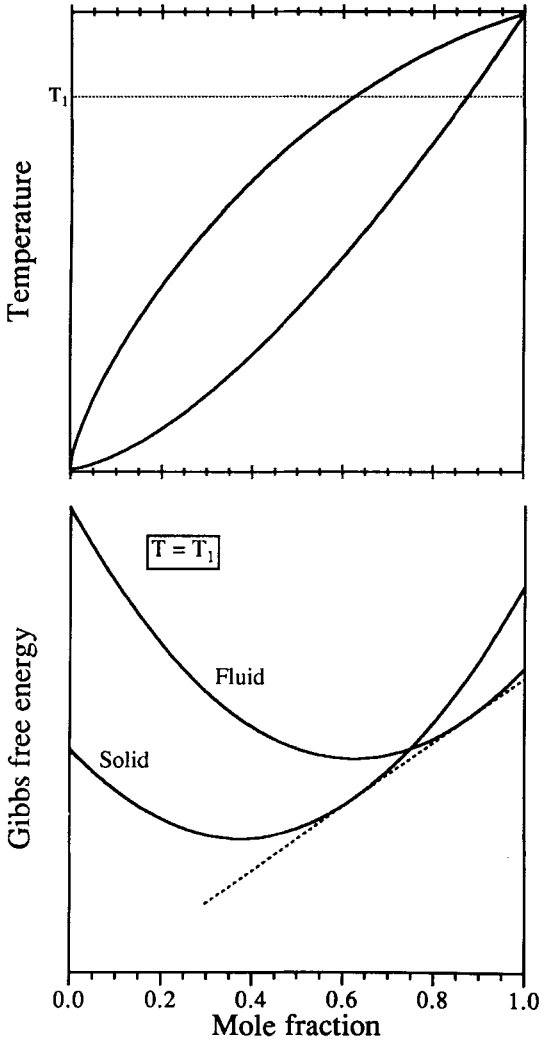

Figure 2 Schematic of construction used to evaluate phase equilibria in the Gibbs representation. The dashed line in the lower figure is tangent to both the fluid- and solid-phase isotherms.

Canonical approach

For a binary mixture in the Gibbs representation, we describe coexistence through reference to a plot — at constant temperature and pressure — of the Gibbs free energy versus mole fraction (Figure 2). At a given composition, the slope of the G vs. x curve and its intercept at $x = 0$ or $x = 1$ can be related to the chemical potentials of each species. Consequently, equality of chemical potentials requires that two coexisting phases share a common tangent in the G-x plane. This construction is displayed in the figures. In the Gibbs representation the *overall* composition is imposed. If this composition falls between the two tangent compositions, the systems splits into two phases. Outside this range, the single stable phase is the one having the lower free energy.

Semigrand approach

The appropriate description of phase equilibria in the semigrand ensemble is made in the $\mu_1 - \xi_2$ plane. Since both of these quantities are field variables, they must be identical in coexisting phases. Thus, coexistence is represented simply by the *intersection* of the two isotherms. For other values of the fugacity fraction ξ_2, the stable phase is again the one which minimizes the thermodynamic potential, in this case μ_1. The construction used to describe coexistence in this representation may be seen in Figure 5, where sample results from this work are analyzed.

One advantage of the semigrand approach is now readily apparent. If the mole fraction is used as an independent variable, the danger exists of choosing a value which lies in the two-phase region. A simulation conducted under such conditions would be prone to error, especially if the chosen composition represented a locally unstable phase, and not one which is at least metastable. In a semigrand simulation this issue presents much less of a problem. Because only field variables are imposed, the system cannot be constrained to an unstable region. At worst, ξ_2 "near" coexistence could be chosen, for which two phases exist of nearly equal stability. A simulation conducted under such conditions may also fluctuate between the two phases; the rate at which these transitions occur depends on the size of the free energy barrier which separates the phases. Except for systems near a critical point (which has never been observed for a fluid–solid transition), it is reasonable to expect that this barrier is large enough to make the transitions very infrequent, if not entirely unobservable. We stress the constrast with the canonical approach, where large fluctuations and interfacial effects are *expected* to govern behavior. As ξ_2 is removed from its coexistence value, the barrier from the metastable side decreases, while that from the globally stable one increases. This trend encourages a system prepared in the metastable state to rapidly move into the stable one, never to return. It should also be noted that the free energy barrier separating the two phases in an extensive quantity, and grows with the system size.

In the present studies of solid–fluid coexistence, these issues have diminished relevance. Because of the single-occupancy constraint, there is no possibility that the system may fluctuate between solid and fluid phases, regardless of their relative stability. This would be true even if we were using the canonical approach. However, when considering solid–solid coexistence (which we do only briefly here), much more caution must be exercised. There are no artificial constraints separating two solid phases, and so the possibility of fluctuation exists. It is in this application that the semigrand approach may prove especially advantageous.

3. EXPERIMENTAL

Isobaric, semigrand Monte Carlo simulations of binary hard sphere mixtures were conducted for three different sphere size ratios $\lambda = \sigma_2/\sigma_1$: 0.95, 0.93, and 0.90. Five hundred spheres were used in each simulation, and the center of each sphere was constrained to its own fcc, Wigner-Seitz (WS) cell [17]. The mechanism for performing a simulation in this ensemble has been described previously [15]. In each simulation, at least 1.5×10^4 and as many as 48.0×10^4 sampling cycles were performed, beyond the equilibration phase. A sampling cycle consisted of one attempted translation per particle, one attempted identity change per particle, and one attempted volume change. Typically, 5.0×10^4 sampling cycles were performed, after an initial 4.0×10^4 relaxation cycles which were not included in the averaging. Five to seven isotherms were generated for each sphere size ratio; these are listed in Table 1. At each temperature, the composition and density were measured for nine fugacity fractions ξ_2: 0.0125, 0.05, 0.10, 0.15, 0.20, 0.30, 0.50, 0.70, 0.90. Two simulations were conducted at each value of ξ_2. These differed in the nature of the initial configuration used to start the simulation — one began from the final configuration of a simulation with a smaller value of ξ_2, while the other started with the final configuration of a simulation of larger ξ_2 (the simulations at $\xi_2 = 0.0125$ and 0.90 began from a perfect crystal of pure 1 and pure 2, respectively). Thus each isotherm was evaluated from two series of simulations, a "forward" set (of increasing ξ_2) and a "reverse" set (of decreasing ξ_2). Comparison of the forward and reverse values for each ξ_2 provided an effective means for determining whether the simulations had converged. In most instances, both simulations were continued if their averages for the mole fraction x_2 differed from each other by more than 0.005, which is the estimated statistical error [18] in the measurements. The observed difference between the forward and reverse values was typically about 0.002.

Only first- and second-nearest neighbor interactions (18 in number) were considered in the $\lambda = 0.95$ simulation, while up to third-nearest neighbors (42 in number) were tested for overlap in the $\lambda = 0.93$ and 0.90 calculations. Occasional tests of all interactions revealed no undetected overlaps. In addition to the moves described above, in each cycle 100 attempts were made to move a particle to a random point in its WS cell (as opposed to moving it within a small region centered on its present position). This type of move was incorporated after discovering that it alleviated a severe ergodic problem that was observed in one simulation very early in this work.

In most simulations, the current configuration was written to tape after every 100–500 cycles for subsequent analysis (to be presented in a future publication). Also, the change in potential with size ratio, $\partial(\beta\mu_1)/\partial\lambda$, was averaged in all simulations using

Table 1 Values of $kT/P\sigma_1^3$ studied at each size ratio λ

$\lambda = 0.95$	$\lambda = 0.93$	$\lambda = 0.90$
0.085	0.085	0.085
0.080	0.080	0.080
0.078	0.076	0.075
0.076	0.072	0.070
0.074	0.068	0.065
0.072		0.060
		0.055

a special but straightforward technique. Since these results were not used in constructing the phase diagram, they too are not reported here.

4. RESULTS

The simulation averages of the mole fraction x_2 and the density $\rho\sigma_1^3$ are presented in Tables 2 and 3. The statistical errors in these results are estimated [18] as 0.003 and 0.01, respectively. The values tabulated are averages of the forward and reverse runs. As indicated in Table 2, in several instances the forward and reverse results could not be brought into agreement, even after very lengthy averaging. Also marked in the table are states that required very long averaging — more than 300,000 cycles — to reach convergence.

The convergence of the composition and the density are illustrated in Figure 3,

Table 2 Mole fraction x_2 averaged over forward and reverse sets of runs

$\lambda = 0.90$	Temperature, $kT/P\sigma_1^3$						
ξ_2	*0.055*	*0.060*	*0.065*	*0.070*	*0.075*	*0.080*	*0.085*
0.0125	0.4188†	0.2805†*	0.2342	0.1937	0.1677	0.1586	0.1428
0.0500	0.8749†	0.8021†*	0.7225	0.6534†*	0.5877	0.5458	0.4877†
0.1000	0.9526†	0.9198	0.8661*	0.8290	0.7890*	0.7448	0.7186†
0.1500	0.9730	0.9463	0.9190	0.8929*	0.8622	0.8333*	0.8110
0.2000	0.9803	0.9614*	0.9478	0.9288	0.8996*	0.8801	0.8576
0.3000	0.9900	0.9819	0.9700	0.9566	0.9416	0.9261	0.9117
0.5000	0.9955	0.9924	0.9862	0.9825	0.9765	0.9717	0.9649
0.7000	0.9995	0.9967	0.9952	0.9925	0.9888	0.9872	0.9839
0.9000	1.0000	0.9993	0.9988	0.9981	0.9973	0.9967	0.9960
$\lambda = 0.93$	Temperature, $kT/P\sigma_1^3$						
ξ_2	0.068	0.072	0.076	0.080	0.085		
0.0125	0.0941	0.0914	0.0838	0.0787	0.0738		
0.0500	0.3567*	0.3291	0.3110*	0.2889	0.2680		
0.1000	0.5735*	0.5481*	0.5132*	0.4885	0.4665		
0.1500	0.7067	0.6693	0.6521†	0.6172†	0.5925		
0.2000	0.7883	0.7592*	0.7346	0.7051	0.6887		
0.3000	0.8760	0.8497	0.8360	0.8167	0.7915†		
0.5000	0.9441	0.9361	0.9256	0.9168	0.9064†		
0.7000	0.9765	0.721	0.9660	0.9635	0.9563		
0.9000	0.9936	0.9932	0.9918	0.9900	0.9891		
$\lambda = 0.95$	Temperature, $kT/P\sigma_1^3$						
ξ_2	0.072	0.074	0.076	0.078	0.080	0.085	
0.0125	0.0563	0.0538	0.0525	0.0498	0.0507	0.0470	
0.0500	0.2005	0.1998	0.1951	0.1908	0.1878	0.1768	
0.1000	0.3707*	0.3598	0.3479	0.3436*	0.3314	0.3213†	
0.1500	0.4868	0.4836	0.4660	0.4592	0.4624	0.4355	
0.2000	0.5880	0.5761*	0.5619	0.5584	0.5525	0.5325	
0.3000	0.7174	0.7106	0.7061	0.6902*	0.6850	0.6672	
0.5000	0.8694	0.8569	0.8558	0.8467	0.8398	0.8283	
0.7000	0.9388	0.9362	0.9330	0.9318	0.9276	0.9190	
0.9000	0.9832	0.9831	0.9821	0.9818	0.9812	0.9788	

* More than 300,000 total (forward plus reverse) simulation cycles needed for convergence.
† Averages from forward and reverse sets differed by more than 0.005.

Table 3 Density $\rho\sigma_1^3$ averaged over forward and reverse sets of runs

$\lambda = 0.90$	Temperature, $kT/P\sigma_1^3$						
ξ_2	*0.055*	*0.060*	*0.065*	*0.070*	*0.075*	*0.080*	*0.085*
0.0125	1.233	1.177	1.151	1.122	1.097	1.085	1.062
0.0500	1.392	1.333	1.275	1.230	1.187	1.159	1.109
0.1000	1.441	1.395	1.331	1.294	1.254	1.207	1.145
0.1500	1.458	1.403	1.357	1.322	1.280	1.242	1.163
0.2000	1.460	1.408	1.378	1.342	1.292	1.259	1.179
0.3000	1.471	1.433	1.390	1.352	1.313	1.274	1.201
0.5000	1.472	1.439	1.392	1.370	1.337	1.310	1.345
0.7000	1.472	1.441	1.415	1.374	1.329	1.311	1.252
0.9000	1.472	1.452	1.417	1.382	1.336	1.315	1.267
$\lambda = 0.93$	Temperature, $kT/P\sigma_1^3$						
ξ_2	0.068	0.072	0.076	0.080	0.085		
0.0125	1.109	1.102	1.083	1.071	1.051		
0.0500	1.149	1.130	1.115	1.093	1.070		
0.1000	1.184	1.167	1.143	1.123	1.103		
0.1500	1.214	1.187	1.172	1.143	1.121		
0.2000	1.237	1.211	1.189	1.161	1.143		
0.3000	1.263	1.231	1.214	1.191	1.156		
0.5000	1.280	1.262	1.237	1.215	1.190		
0.7000	1.292	1.271	1.241	1.229	1.191		
0.9000	1.290	1.283	1.258	1.226	1.211		
$\lambda = 0.95$	Temperature, $kT/P\sigma_1^3$						
ξ_2	0.072	0.074	0.076	0.078	0.080	0.085	
0.0125	1.098	1.086	1.077	1.063	1.068	1.048	
0.0500	1.102	1.099	1.093	1.086	1.080	1.059	
0.1000	1.129	1.118	1.106	1.101	1.086	1.073	
0.1500	1.136	1.134	1.117	1.110	1.113	1.084	
0.2000	1.153	1.143	1.130	1.127	1.121	1.100	
0.3000	1.170	1.163	1.158	1·141	1.136	1.113	
0.5000	1.205	1.184	1.183	1.166	1.155	1.134	
0.7000	1.210	1.201	1.192	1.186	1.172	1.143	
0.9000	1.214	1.210	1.199	1.199	1.190	1.160	

where the running averages of x_2 and $\rho\sigma_1^3$ are shown for the two most extreme cases. Plots are presented for $\lambda = 0.95$, $T^* = 0.085$, the highest temperature (*i.e.*, lowest pressure) simulated, and for $\lambda = 0.90$, $T^* = 0.055$, the lowest temperature (highest pressure) simulated; forward and reverse sets are shown separately. We expect the rate of convergence to be much more rapid in the $\lambda = 0.95$ system, and this indeed what we observe. In fact, for the $\lambda = 0.90$ case the forward and reverse simulations do not come into agreement, but instead level off at different densities and compositions.

In Figure 4 is plotted the integrand needed in Equations (7) and (8), as a function of fugacity fraction. Only the results for $\lambda = 0.90$ are shown; the figures for the other size ratios are qualitatively the same, although the $\xi_2 = 0$ intercepts are much smaller. The results from the forward and reverse sets of the $T^* = 0.055$ isotherm are in substantial disagreement, and thus are shown separately. These curves were fit to bicubic splines (as a function of T^* and ξ_2) and integrated according to Equation (8) to determine $\beta\mu_1$; the pure species-2 reference chemical potential $\beta\mu_2^0$ was computed from the data of Hoover and Ree [13]. A check of the integration was performed by evaluating $\beta\mu_1$ ($\xi_2 = 0$) according to Equation (8), and comparing this result with that

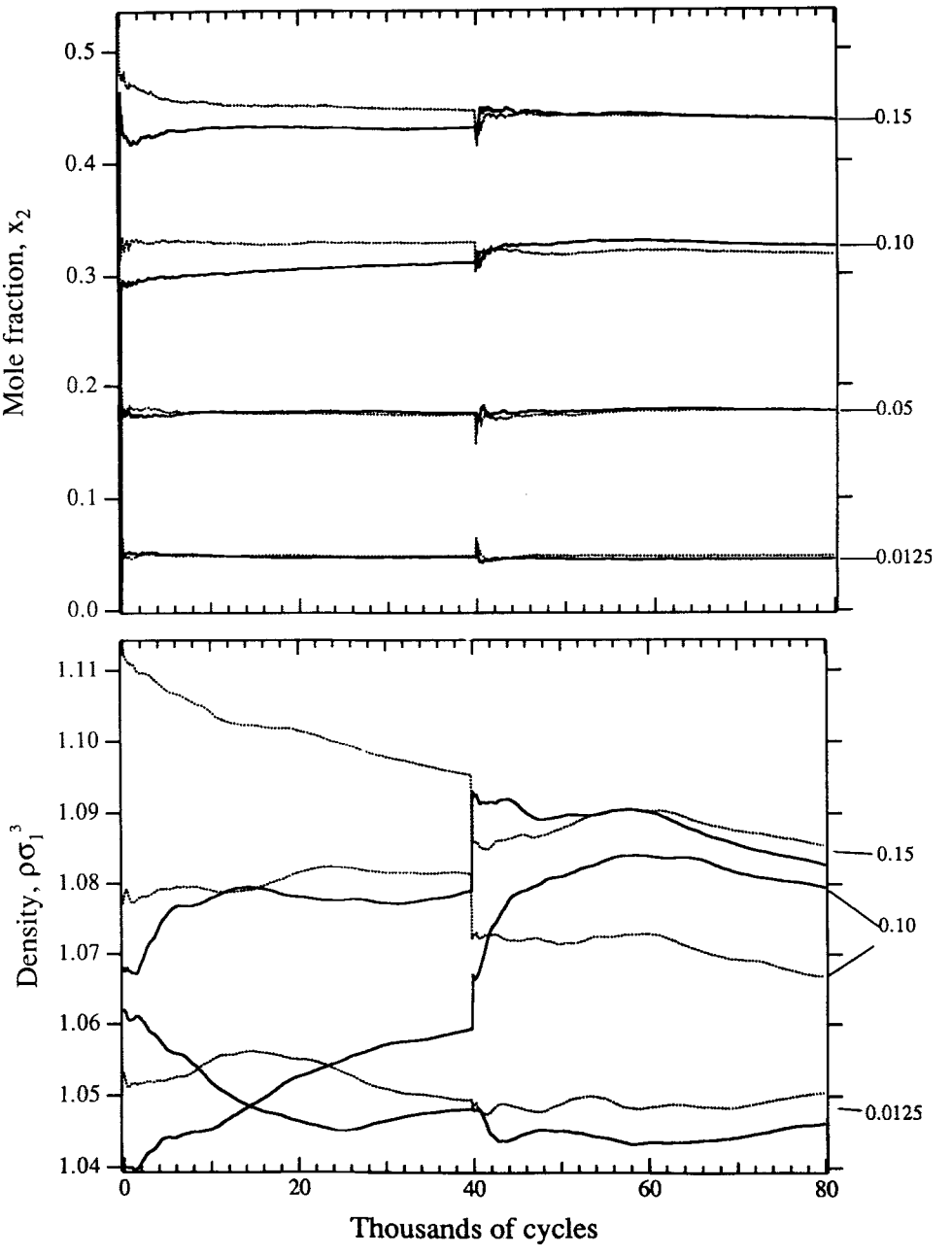

Figure 3a Running averages of the composition and density. $\lambda = 0.95$, $T^* = 0.085$. The fugacity fraction ξ_2 is indicated to the right of the figures. The solid lines are from the forward set of simulations, and the dashed lines are from the reverse set. The equilibration phase ends at 40,000 cycles, causing the abrupt jump seen in the figures at this point.

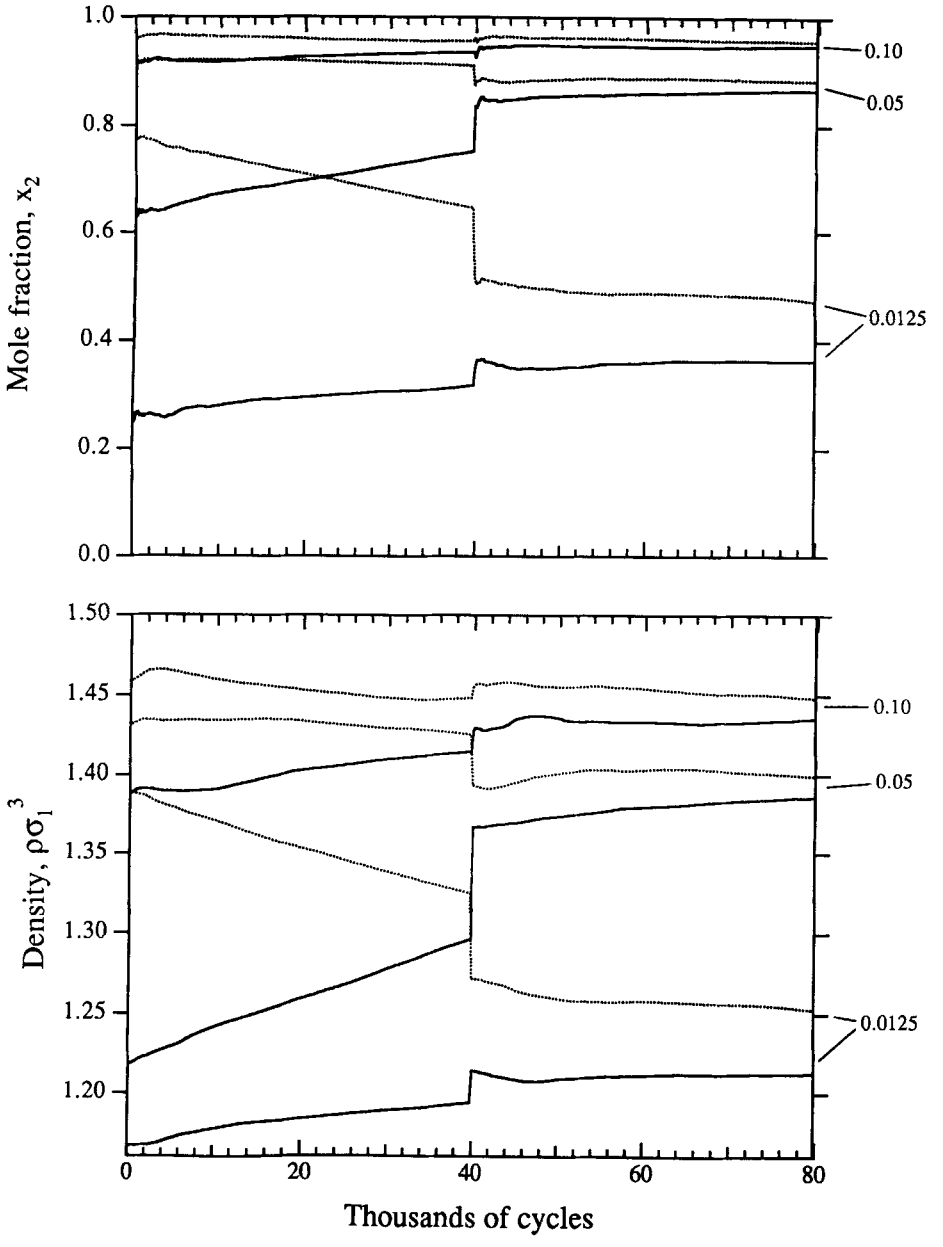

Figure 3b Running averages of the composition and density. $\lambda = 0.90$, $T^* = 0.055$. The fugacity fraction ξ_2 is indicated to the right of the figures. The solid lines are from the forward set of simulations, and the dashed lines are from the reverse set. The equilibrium phase ends at 40,000 cycles, causing the abrupt jump seen in the figures at this point. Note the difference in the scale at the density plots for (a) and (b).

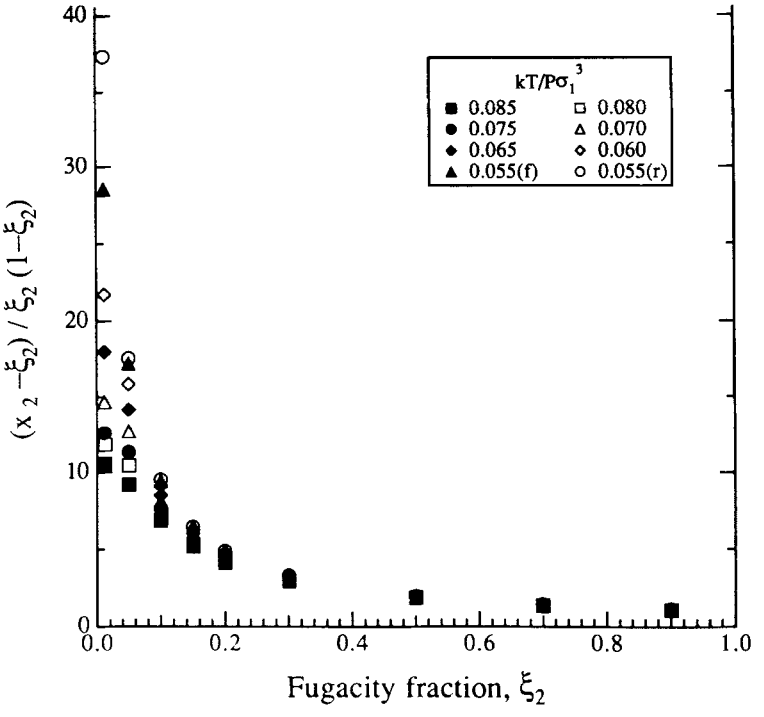

Figure 4 Integrand seen in Equation (7) and (8), for $\lambda = 0.90$ mixture. The two curves for $T^* = 0.055$ are from the forward and reverse sets of simulations, respectively.

of Hoover and Ree. The comparison was always within the statistical errors reported by them, even for the interpolated temperatures.

The calculation performed to determine coexistence is illustrated in Figure 5, where we plot the $T^* = 0.060$ isotherms of the fluid and solid compositions and free energies for the $\lambda = 0.90$ system. The fluid-phase properties were evaluated using the semi-empirical equation of state of Mansoori, *et al.* [19]. The figure shows how little the fluid and solid free energies differ when compared to the difference between the pure-1 and pure-2 free energies. Nevertheless, we may with confidence compare $\beta\mu_1$ for the fluid and solid phases. Our integral check indicates that the error in $\beta\mu_1$ (solid) is no greater than 0.008, which is less than the statistical error of 0.015 reported by Hoover and Ree for the pure fluid chemical potentials. Although the coexisting phases are rich in species 2, the fugacity fraction of the transition is small — of the order 0.01 to 0.10 — and so we need not integrate our results very far to reach coexistence; thus our actual error should be less than that indicated by the integral check. The error introduced by use of the equation of state to describe the fluid phase should be noted, as it too may be larger than that of our simulations, or even that of the Hoover and Ree's results.

Coexistence occurs where the difference in fluid and solid free energies is zero. An expanded view of the transition region is also included in Figure 5, with the fluid and solid mole fractions superimposed. Once the transition value of ξ_2 is determined, the composition plots may be read to evaluate the compositions the coexisting phases. All

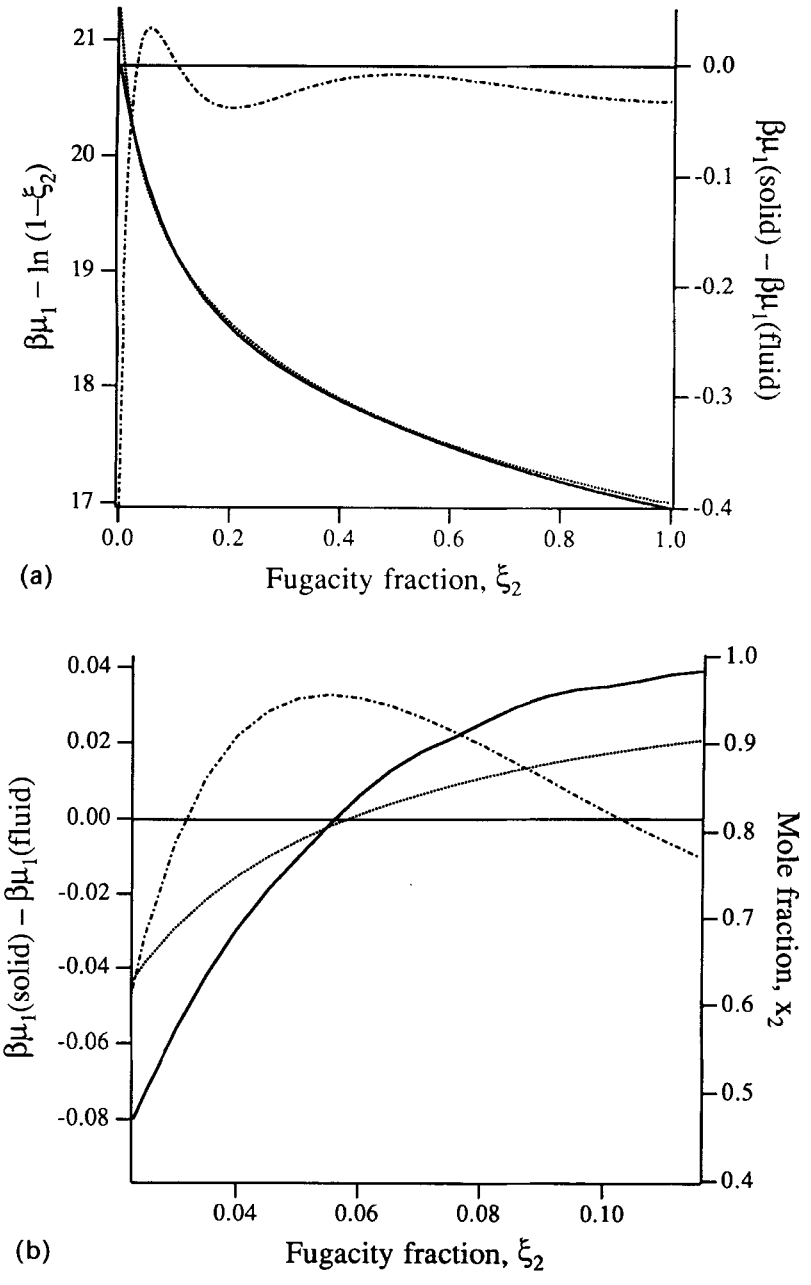

Figure 5 Stability plots of the fluid and solid phases. The solid curve represents the solid phase, and the dashed one the fluid phase. (a) Coexistence. The abscissa on the left is chosen instead of $\beta\mu_1$ itself because it is well behaved for all ξ_2, and yet can still be used to evaluate coexistence in the same way that $\beta\mu_1$ can. The curve plotted on the right can be used with the zero line to see the transition more easily. The double crossing indicates an azeotrope. (b) Composition averages are superimposed with the coexistence curve and zero line seen in (a).

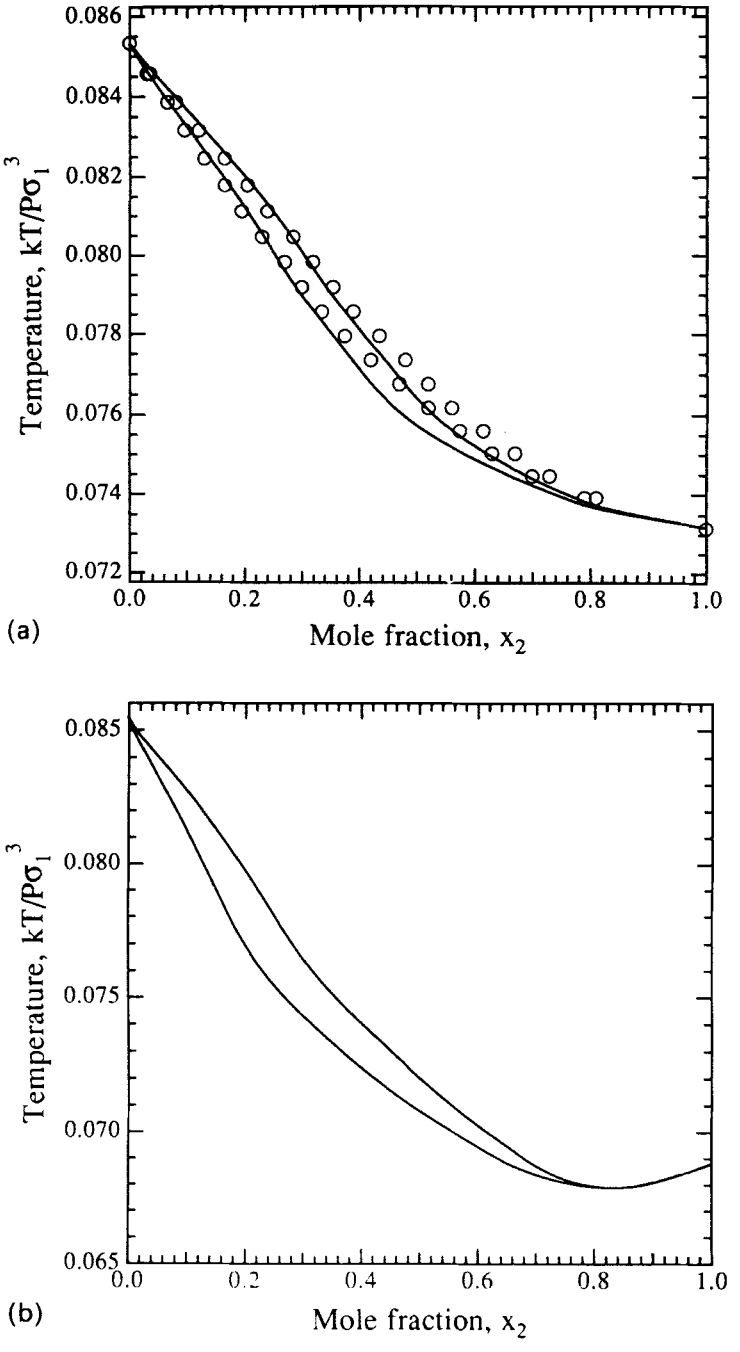

Figure 6 Phase diagrams for three mixtures: (a)$\lambda = 0.95$; (b)$\lambda = 0.93$; (c)$\lambda = 0.90$. The solid lines are results from this work, and the circles represent the data of Kranendonk and Frenkel.

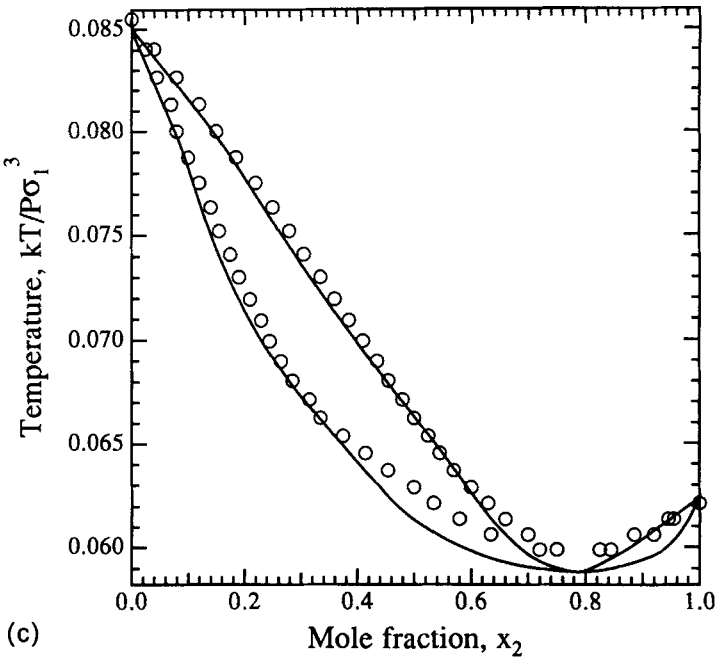

Figure 6 (*Continued*)

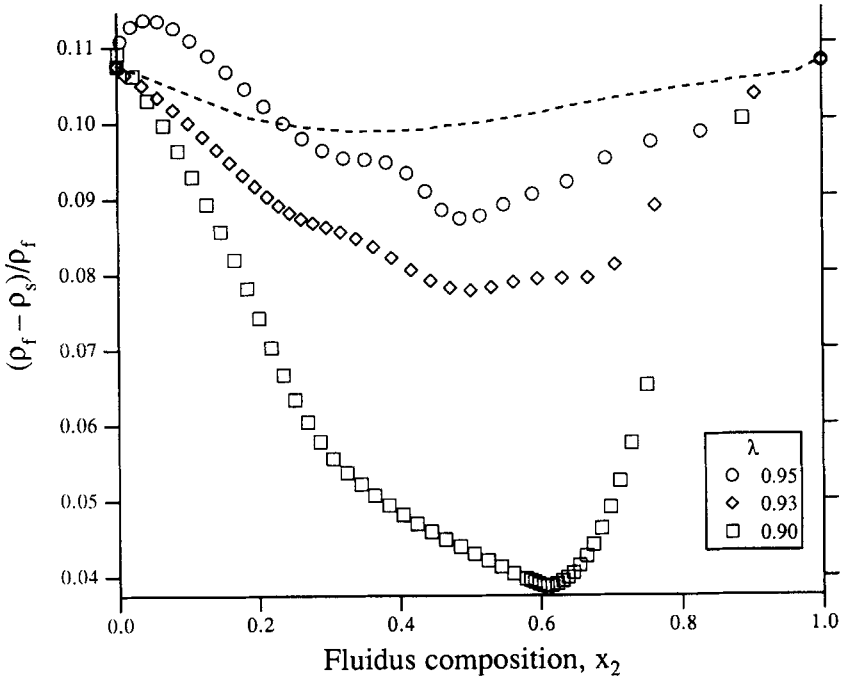

Figure 7 Relative density change of freezing. The open points are simulation results from the present work, and the dashed line represents the results of Kranendonk and Frankel for the $\lambda = 0.95$ mixture.

of these computations were accomplished using the bicubic spline fits of $(x_2 - \xi_2)/\xi_2(1-\xi_2)$. Phase diagrams for the three mixture types are presented in Figure 6. In all but one instance, the solid-phase properties were determined by averaging results from the forward and reverse sets of simulations. The exception is the $\lambda = 0.90$, $T^* = 0.055$ isotherm, which was described using only the forward set of results. These results satisfied the integral consistency test much better than did the reverse set, or than did the average of the two.

The $\lambda = 0.95$ system displays a spindle-type diagram, while azeotropes are observed in the $\lambda = 0.93, 0.90$ mixtures. The conditions at the azeotypes are: $\lambda = 0.93$, $T^* = 0.0678$, $x_2 = 0.0834$; $\lambda = 0.90$, $T^* = 0.0587$, $x_2 = 0.79$. We performed a comparison of the stability — as given by $\beta\mu_1$ — of the states sampled by the forward sets (integrated from a pure-1 reference) and reverse sets (integrated from a pure-2 reference) of simulations, and found solid–solid coexistence very close to the azeotropic temperature. However, this transition is tenuous, and can be made to disappear by shifting $\beta\mu_1$ within its estimated error. Consequently, we are not prepared to conclude here that it exists.

The final quantity we present is the density change of the transition, which is plotted as a function of the coexistence fluid mole fraction in Figure 7.

5. DISCUSSION

For two of the systems, $\lambda = 0.95$ and $\lambda = 0.90$, we were able to compare our results with those of Kranendonk and Frenkel [12]. These comparisons are included in the figures. Overall, the agreement is satisfactory, although some significant differences are apparent. The phase diagrams are in good agreement, especially at high temperature. The divergence at low temperature for the $\lambda = 0.95$ system is quite small and, if not a result of statistical error inherent in the simulations, is likely due to the difference in system size used for the two studies. The disagreement for the $\lambda = 0.90$ system is more substantial. We find the azeotrope at a lower temperature (higher pressure) than do Kranendonk and Frenkel, although the azeotropic composition is in perfect agreement. Given the sensitivity of the transition in this region to small changes in the chemical potential (cf. Figure 5), this discrepancy is not surprising. It too may be attributed to the difference in system size of the simulations, or possibly to Kranendonk and Frenkel's use of their own simulation data for the fluid phase, which are certain to be more accurate than the equation of state used here. The comparison of the relative density change of freezing for the $\lambda = 0.95$ system is unsatisfactory, and we can offer no explanation for the large disagreement between our result and that of Kranendonk and Frenkel. However, we note that they do agree qualitatively — both show that the density change decreases as the fluidus composition tends toward equimolar. This trend is significant because it contradicts the conclusion of some implementation of density functional theory [5,6].

For the $\lambda = 0.90$ mixture, we believe that the very slow convergence of the forward and reverse simulation averages — as demonstrated in Figure 3 and by the concentration of highlighted entries in Table 2 — is very convincing evidence for the existence of a second, metastable solid phase at the lowest of the temperatures examined here. However, we are unable to demonstrate solid–solid coexistence, with any certainty. Kranendonk and Frenkel report that a eutectic is formed for $\lambda < 0.0875$. We find that, while maybe not present, a eutectic is imminent at $\lambda = 0.90$. Thus, although we cannot verify or disprove their claim, our results support its plausibility.

6. SUMMARY AND CONCLUSIONS

We have demonstrated that the semigrand approach can be used to evaluate fluid–solid coexistence, and argue that it has distinct advantages over constant-composition, canonical methods for evaluating solid–solid equilibria. It provides a means for mapping out a complete thermodynamic description of a mixture without danger of stimulating a two-phase system. Moreover, by using the method to relate two pure phases of known properties, the correctness of the computations may be verified. The methodology is easily extended to mixtures of any number of components.

We studied the fluid–solid coexistence properties of binary hard sphere mixtures of three size ratios $\lambda = \sigma_2/\sigma_1$. For $\lambda = 0.95$, a spindle-type diagram was observed, while azeotropes were seen in $\lambda = 0.93$ and $\lambda = 0.90$ mixtures. Metastable solid states are in evidence for the $\lambda = 0.90$ system at low temperatures (high pressures), but we are unable to conclude that solid–solid coexistence is present at the conditions studied.

Finally we remark that the semigrand formalism may also be of value when employed in density functional approaches. Two general schemes are currently in use, one canonical in nature, and the other grand canonical. With the first method, the composition and pressure are specified, and the crystal free energy is estimated as a function of the density and crystal structure. This free energy is then minimized with respect to these variables to yield the properties of the most stable solid. This approach further requires that numerical derivatives of the minimized free energy be taken to evaluate the chemical potentials needed to find coexistence (or equivalently, to perform the double-tangent construction). The numerical operation is inconvenient at best, and highly prone to error at worst. In contrast, the grand canonical approach specifies the mixture volume and species chemical potentials. The approximate solid free energy is minimized to determine the density and composition (as well as the crystal structure), while the pressure is easily found from the minimum value of the free energy. Consequently, no numerical differentiation is required to evaluate any thermodynamic properties. The only problem with the approach is that no "standard" thermodynamic properties, *i.e.* the pressure or composition, can be specified *a priori*, so it is difficult to construct hard sphere "isotherms" (really isobars). While this is no more than an inconvenience, it is one that is not present in a semigrand approach. Here we specify the pressure and the fugacity fraction, and find the density and composition by minimizing the approximate free energy, the value of which yields μ_1 directly. The species-2 chemical potential then follows directly from ξ_2.

Acknowledgements

This work was supported by the U.S. National Science Foundation under Grant No. CTS-8909365, and through the Presidential Young Investigator program. The author is grateful to Robert Richard for programming assistance provided in the initial stages of this work, and to A.D.J. Haymet for his interest and advice.

References

[1] A.D.J. Haymet, "Freezing and interfaces: Density functional theories in two and three dimensions", *Prog. Sol. State Chem.*, **17**, 1 (1986).
[2] A.D.J. Haymet, "Theory of the equilibrium liquid-solid transition", *Ann. Rev. Phys. Chem.*, **38**, 89 (1987).
[3] M. Baus, "Statistical mechanical theories of freezing: An overview", *J. Stat. Phys.*, **48**, 1129 (1987).
[4] X.C. Zeng and D.W. Oxtoby, "Density functional theory for freezing of a binary hard sphere liquid", *J. Chem. Phys.*, **93**, 4357 (1990).

[5] J.L. Barrat, M. Baus and J.P. Hansen, "Density-functional theory of freezing of hard sphere-mixtures into substitutional solid solutions", *Phys. Rev. Lett.*, **56,** 1063 (1986).
[6] J.L. Barrat, M. Baus and J.P. Hansen, "Freezing of binary hard sphere mixtures into disordered crystals: a density functional approach", *J. Phys. C.: Solid State Phys.*, **20,** 1413 (1987).
[7] H. Xu and M. Baus, "The partial freezing of hard sphere mixtures", *J. Phys. C.: Solid State Phys.*, **20,** L373 (1987).
[8] S.L. Smithline and A.D.J. Haymet, "Density functional theory for the freezing of 1:1 hard sphere mixtures", *J. Chem. Phys.*, **86,** 6486 (1987).
[9] S.W. Rick and A.D.J. Haymet, "Density functional theory for the freezing of Lennard-Jones binary mixtures", *J. Chem. Phys.*, **90,** 1188 (1989).
[10] X.C. Zeng and D.W. Oxtoby, "Density functional theory for freezing of a binary hard sphere liquid", *J. Chem. Phys.*, **93,** 4357 (1990).
[11] A.R. Denton and N.W. Ashcroft, "Weighted-density-functional theory of nonuniform fluid mixtures: Application to freezing of binary hard-sphere mixtures", *preprint*, (1990).
[12] W.G.T. Kranendonk and D. Frenkel, "Computer simulation of solid-liquid coexistence in binary hard sphere mixtures", *J. Phys.: Condens. Matter*, **1,** 7735 (1989).
[13] W.G. Hoover and F.H. Ree, "Melting transition and communal entropy for hard spheres", *J. Chem. Phys.*, **49,** 3609 (1968).
[14] J.B. Briano and E.D. Glandt, "Statistical thermodynamics of polydisperse fluids", *J. Chem. Phys.*, **80,** 3336 (1984).
[15] D.A. Kofke and E.D. Glandt, "Monte Carlo simulation of multicomponent equilibria in a semigrand canonical ensemble", *Mol. Phys.*, **65,** 1105 (1988).
[16] A.Z. Panagiotopoulos, "Direct determination of phase coexistence properties of fluids by Monte Carlo simulation in a new ensemble", *Mol. Phys.*, **61,** 813 (1987).
[17] The algorithm for evaluating whether a sphere is within its WS cell is very simple: if Δx, Δy, and Δz measure the displacement of the center of a sphere from the center of its fcc cell in the x,y, and z directions, respectively, then the center of the sphere is within the cell if all of the following conditions hold: $|\Delta x| + |\Delta y| < D$;$|\Delta x| + |\Delta z| < D$; and $|\Delta y| + |\Delta z| < D$; where D is $\sqrt{2}$ times one-half the nearest neighbor separation, and $|\ldots|$ indicates the absolute value.
[18] J. Kolafa, "Autocorrelations and subseries averages in Monte Carlo simulations", *Mol. Phys.*, **59,** 1035 (1986).
[19] G.A. Mansoori, N.F. Carnahan, K.E. Starling and T.W. Leland Jr., "Equilibrium thermodynamic properties of the mixture of hard spheres", *J. Chem. Phys.*, **54,** 1523 (1971).